FEBS Letters 346 (1994) 32–38

FEBS 13912

Minireview

Structure, transmembrane topology and helix packing of P-type ion pumps

David L. Stokes[a,*], William R. Taylor[b], N. Michael Green[b]

[a]*Department of Molecular Physiology and Biological Physics, Box 449, University of Virginia Health Sciences Center, Charlottesville, VA 22908, USA*
[b]*Laboratory of Mathematical Biology, National Institute for Medical Research, Mill Hill, London NW7 1AA, UK*

Received 15 March 1994

Abstract

Electron microscopy has recently provided improved structures for P-type ion pumps. In the case of Ca^{2+}-ATPase, the use of unstained specimens revealed the structure of the transmembrane domain. The composition of this domain has been controversial due to the variety of methods used to study the number and exact locations of transmembrane crossings within the sequence. After reviewing the results from several members of the family, we found a consensus for 10 transmembrane segments, and also that 10 helices fitted well into the structure of Ca^{2+}-ATPase. Thus, we present the most detailed model for transmembrane structure so far, in the hope of stimulating more precise experimental strategies.

Key words: Ion transport; Membrane domain; Protein structure; Protein folding; Ca^{2+}-ATPase; Na^+/K^+-ATPase

1. Introduction

Integral membrane proteins are difficult to crystallize and only a few high-resolution structures are known. Our only structural clues to mechanisms of ion transport come from bacteriorhodopsin, for which an atomic structure has been deduced by electron crystallography [1]. Mechanisms for P-type ion pumps are based mainly on kinetic studies, mutagenesis, affinity labelling and analysis of sequences. Although there are no foreseeable prospects for an atomic structure for these pumps, there has been recent progress in structure determination by electron microscopy with prospects for a structure at 6 Å resolution. In this review, we discuss some recent work on the structure of Ca^{2+}-ATPase and Na^+/K^+-ATPase, summarize the numerous attempts to determine the transmembrane topology of P-type pumps, and use the emerging consensus to model the transmembrane structure of Ca^{2+}-ATPase.

2. Electron microscopic structure determination

Skriver et al. were the first to report crystallization of a P-type pump [2], using vanadate to induce 2D crystals within purified membrane fragments of Na^+/K^+-ATPase. Similar conditions were used by Dux and Martonosi to induce a similar crystal form of Ca^{2+}-ATPase in sarcoplasmic reticulum vesicles [3]. These crystal forms lead to several 3D reconstructions at 25–35 Å resolution of negatively stained Ca^{2+}-ATPase [4,5] and Na^+/K^+-ATPase [6–9]. Thus, the general shape of the cytoplasmic domain of Ca^{2+}-ATPase has been well established and its mass distribution across the sarcoplasmic reticulum membrane has been determined by low-angle, X-ray diffraction [10]. Reconstructions of vanadate-induced crystals of Na^+/K^+-ATPase [6–9] have generally been at lower resolution and the expected similarities between the subunit and Ca^{2+}-ATPase have therefore been difficult to recognize; also, identification of the α subunit of Na^+/K^+-ATPase has not been possible.

Additional crystal forms have been discovered both for Ca^{2+}-ATPase and for Na^+/K^+-ATPase and offer opportunities for higher resolution structures. In the case of Na^+/K^+-ATPase, a recent structure at ~ 25 Å resolution has come from negatively stained crystals induced with $Co(NH_3)_4ATP$ [11]; the resulting molecule bears a reasonable resemblance to Ca^{2+}-ATPase, but there are still uncertainties about the precise location of the membrane and identification of the β subunit. Answers to these important questions require larger crystals and the use of frozen-hydrated, unstained specimens for electron microscopy. Indeed, the most recent crystals of Na^+/K^+-ATPase, grown at low pH (4.8), contain larger, better ordered arrays [12] and it may be possible to study them by these methods. In the case of Ca^{2+}-ATPase, the most recently discovered crystal form requires sub-solubilizing concentrations of detergent [13], which allows molecules to insert into both sides of the bilayer; as a result, the bilayers stack to form multilamellar crystals [14]. Although not ideal for 3D reconstruction by electron microscopy, unstained, frozen-hydrated crystals diffract to 4 Å [15] and the stacking has been shown to be well ordered, both in side views of small crystals and in large flat crystals tilted to 30° (Stokes and Toyoshima, unpub-

* Corresponding author.

SSDI 0014-5793(94)00297-9

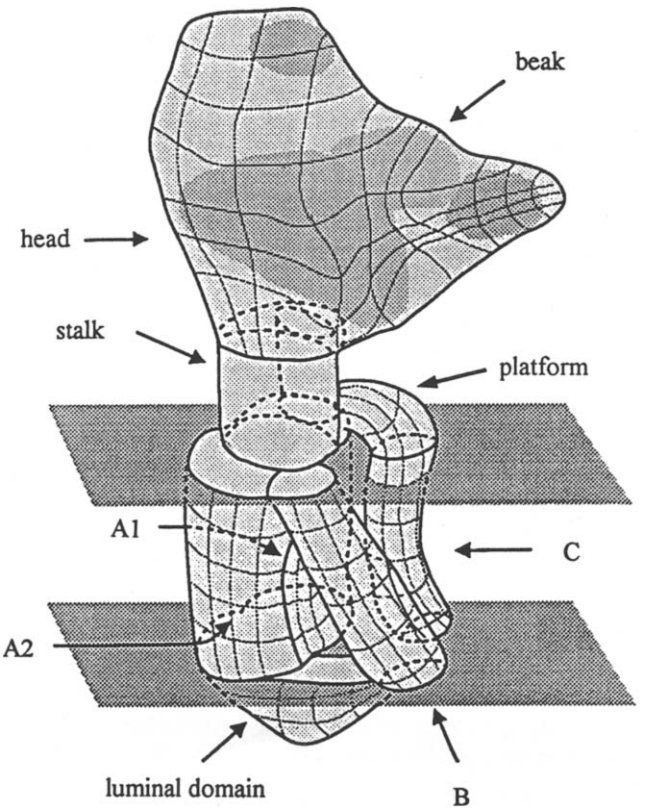

Fig. 1. Cartoon of the structure of Ca^{2+}-ATPase as determined by electron microscopy at 14 Å resolution. The surface of the bilayer is indicated by the two shaded planes; the cytoplasmic side is on top and the luminal (equivalent to extracellular) side is below. The large cytoplasmic part has three distinct components, though smaller domains can be distinguished in the reconstruction. The lumenal part appears as a single small domain. The transmembrane part consists of three distinct lobes labelled A, B, and C; the A lobe was further subdivided into A1 (lying beneath the stalk) and A2 (lying to one side of the stalk). Reprinted with permission from *Nature* [17].

lished results). Thus, there is hope for a higher resolution structure of Ca^{2+}-ATPase, e.g. ~ 6–8 Å. In addition to providing a structure in which helices could be directly observed, comparison of this structure with that from vanadate-induced crystals could reveal structural changes induced by Ca^{2+}-activation of the enzyme. This conformational difference had been suspected based on crystallization requirements [3,13] and recent, explicit studies of crystallization have more precisely defined the conformation as $E_1 \cdot Ca_2$ in multilamellar crystals and E_2 or $E_2 \cdot ATP$ in vanadate-induced crystals [16].

The most informative structure so far has come from a recent reconstruction of vanadate-induced crystals of Ca^{2+}-ATPase in the frozen-hydrated, unstained state [17]. Like a previous attempt with frozen-hydrated specimens [18], the helical symmetry of these tubular crystals was used for reconstruction, but unlike this previous attempt, four crystals were averaged and the resolution was much improved (14 Å). As a result, the bilayer is clearly visible and domains of Ca^{2+}-ATPase can be delineated both inside and outside this bilayer (Fig. 1). Comparison of this structure to the extensive predictions that have been made on the basis of sequence, mutagenesis, and labelling by substrate analogues generated some speculative assignments of several features in the structure, though these assignments remain to be confirmed by other means. Unfortunately, a resolution of 14 Å is too low to resolve individual helices, so we still have no direct evidence for their number or their arrangement in the transmembrane domain.

3. Topology of the membrane domain by indirect means

The similarity between the sequences of the cytoplasmic domains of the P-type ion pumps is in the range of 30–60% and suggests a common fold. Although the predicted transmembrane segments show only slight similarity in individual amino acids (~ 20%), the overall patterns of hydrophobicity are sufficiently similar to imply a common arrangement of transmembrane segments. In

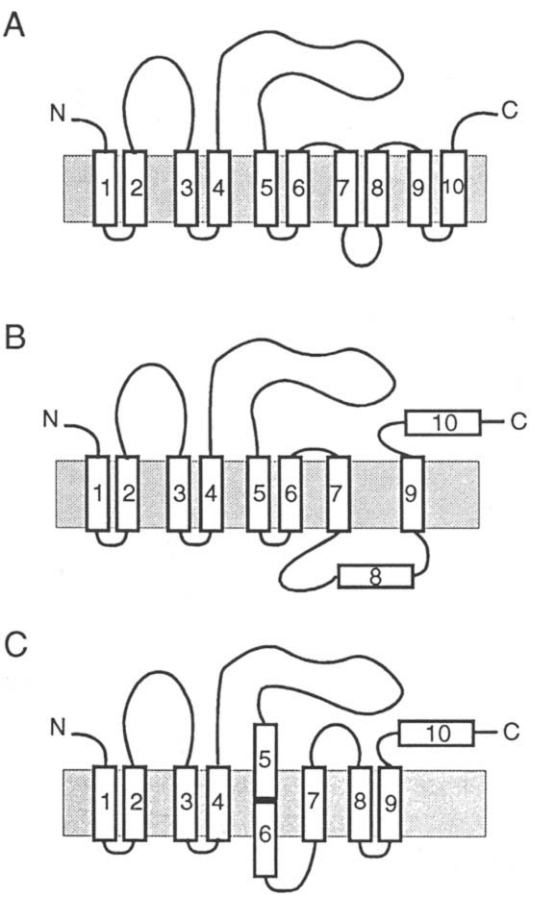

Fig. 2. Three different arrangements for the transmembrane segments of P-type ion pumps. The numbering of segments is based on the 10-segment model taken from reference 19. This is not a comprehensive list of proposed topologies, rather a comparison of three of the more popular arrangements with both C and N termini on the cytoplasmic side of the membrane.

spite of this, widely different interpretations of the hydrophobicity have been made, leading to models with between 7 and 12 segments (Fig. 2), and only recently has experimental evidence emerged to distinguish between them. It is most convenient to discuss this evidence in terms of the ten-segment model first proposed for Ca^{2+}-ATPase (Fig. 2a) based on hydrophobicity analysis [19].

On the one hand, the first four segments are clearly defined in all the pumps. There is no evidence inconsistent with two hydrophobic hairpins in this region (M1-M2 and M3-M4) with a cytoplasmic domain of ~ 150 residues between the hairpins (Fig. 2 and Table 1). The second hairpin (M3-M4) is followed by the major cytoplasmic domain of ~ 450 residues containing conserved sites of phosphorylation and nucleotide binding. On the other hand, the C-terminal portion of the molecule has been more problematic. Of the six C-terminal segments, M8 and M10 are the least hydrophobic and, if these were to be assigned to the lumen and cytoplasm respectively, an eight segment model would result (Fig. 2b). The other main source of uncertainty is the shortness of the M5-M6 hairpin if one excludes the polar N terminus of M5. Indeed, many models for Na^+/K^+-ATPase assign only one transmembrane segment to this region, thus inverting the topology of the subsequent segments (e.g. Fig. 2c).

Attempts to distinguish these models experimentally have been based on a variety of techniques to identify the loops exposed on the cytoplasmic or extracellular faces of the membrane. These include the use of impermeant chemical reagents, proteases, antipeptide antibodies, anti-pump antibodies against subsequently mapped epitopes and, finally, the expression of fusion proteins. In order to facilitate comparisons between the varied methods applied to the different pumps, we considered the results on a loop-by-loop basis rather than comparing models deduced by the various investigators. For each loop, the evidence for or against a cytoplasmic location is summarised in Table 1. No single study is definitive, given the pitfalls of individual experimental techniques, but a consensus can be developed by considering the results en masse.

The L56 loop is very short and lacks polar residues, offering little in the way of epitopes or sites for proteolysis. The only direct evidence for its location comes from the labelling of a cysteine in or near this loop of the H^+/K^+-ATPase by omeprazole or pantoprazole, reagents which are strictly confined to the lumenal surface [41,42]. This is strong evidence for two segments rather than one in this region and this conclusion is further supported by most of the evidence on the location of the next loop, L67. This consists of a number of proteolytic experi-

Table 1
Summary of published evidence for cytoplasmic or luminal location of loops

	Loop 1–2		Loop 3–4		Loop 5–6		Loop 6–7		Loop 7–8		Loop 8–9		Loop 9–10		C-term	
	cyt	lumen	cyt	lumen	cyt	lumen	cyt	lumen	cyt	lumen	cyt	lumen	cyt	lumen	cyt	lumen
SR Ca^{2+}-ATPase																
protease		20		20			20–22,25					20		20		
epitopes										21,24,25					23	
NA^+/K^+-ATPase																
protease							26,27								33	
epitopes		29		37			30,31	28,29	(28)	29,31		30		30	31,32	28
labels		35,36								36					34	
H^+/K^+-ATPase																
protease		41		41		41	41			41	41		41		44	
epitopes										38,39					38	
labels		40				41,42				41						
fusion proteins		43		43		43	43			43	43			43		
Mg^{2+}-ATPase																
fusion proteins		47		47		47	47 2 fusions	47 1 fusion		47	47			47	47	
PM Ca^{2+}-ATPase																
epitopes		46													45	
H^+-ATPase																
protease															48,49	
antibodies															48	

Numbers in the table correspond to papers employing the techniques listed in the left-hand column.

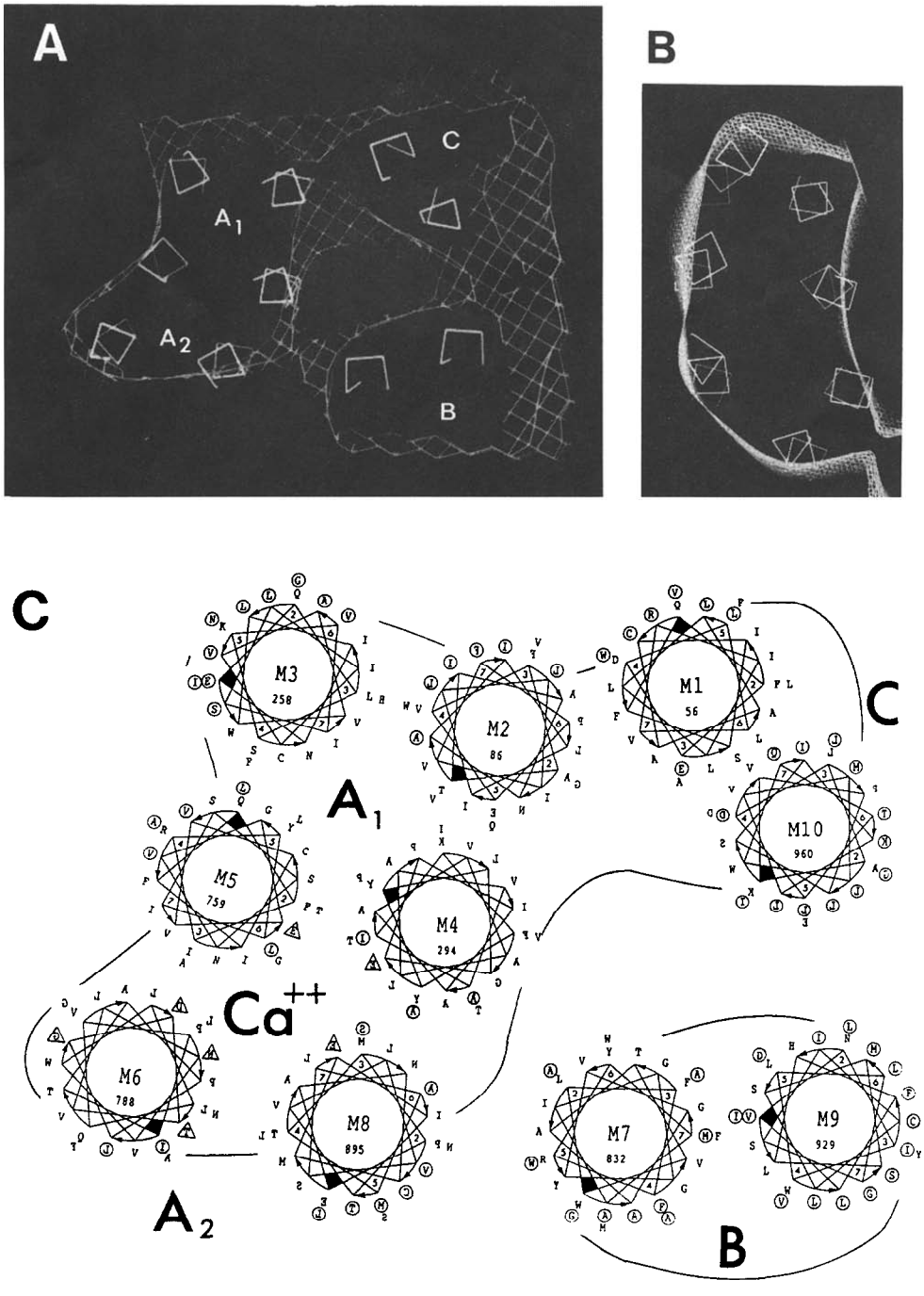

Fig. 3. Hypothetical packing of 10 transmembrane helices. (A). Fitting of 10 helices into the transmembrane domain of Ca^{2+}-ATPase determined by electron microscopy at 14 Å resolution. This view is normal to the membrane surface and the net corresponds to the molecular boundary obtained for ~ 100% volume recovery for the entire molecule. The distance between lines in this net is 2 Å. The transmembrane lobes A1, A2, B and C are the same as Fig. 1. Helices have been placed at the edges of the density based on observations of bacteriorhodopsin reduced to ~ 15 Å resolution, shown in B. This low resolution map of bacteriorhodopsin was generated by applying a temperature factor of 2070 to the structure factors used in reference 1 and the positions of the helical backbones are those determined by the high resolution structure presented therein (structure factors and model courtesy of Richard Henderson). (C) Azimuthal arrangement of these 10 transmembrane helices. The helical wheels, taken from Green [50], were redrawn in accordance with their probable orientation. They are viewed from the cytoplasmic surface so that the odd numbered helices run away from, and even numbered ones (mirrored letters) run towards the viewer. The N-terminal residue of each helix is marked (◆) and its number appears in the center. Around the periphery, the numbers 2–7 designate the remainder of the first heptad of the helix. Each numbered residue is linked to the corresponding residue of succeeding heptads by the curved arrows. The variable sites (○) were defined by minima in the plots of mean pairwise identity within a family of nine Ca^{2+} pumps. Residues which are thought to contribute to the Ca^{2+} site [54] are also marked (△). Because at least 23 residues are shown for each helix, the N and C termini overlap and are shown by doubled residues with the C-terminal ones at higher radius. The main transmembrane masses are designated A_1, A_2, B, and C as in Figs. 1 and 3a.

ments from different laboratories showing cleavage from the cytoplasmic side [20–22,25–27,41] and two sets of experiments with antibodies [30,31]. The only conflicting evidence (discussed further below) arose from use of one monoclonal antibody against Na^+/K^+-ATPase [28,29] and an anomalous result from a fusion protein [47].

The L78 loop is the longest extracellular segment (35 residues) and it is immunologically the most reactive. At least six independent sets of experiments on four different pumps assign this loop to the extracellular surface [21,24,25,29,31,36,38,39]. Only one antibody suggested a cytoplasmic location [28] and immunogold labelling [29] has recently shown this same antibody to bind on the extracellular surface.

Immunogold labelling [29] has also been used to re-evaluate the location of the antibody to the interface between M6 and L67 [28] and, in this case, the extracellular location of this antibody was confirmed. It is difficult to reconcile this result with numerous others relating to this loop, but the authors favored a model in which a large segment from the middle of M6 to the beginning of M8 was extracellular. Because a different antibody to an overlapping epitope has been found to bind to the cytoplasmic surface [31], and because there are also conflicts with results from proteolysis [26,27] and epitope insertion [30], further characterization of this antibody is desirable. Possibly the cytoplasmic epitope was inaccessible (as was observed for L67 of Ca^{2+}-ATPase [22,25]) and the observed binding was due to a cross-reacting epitope on the extracellular surface.

The evidence for the location of the C-terminus in the cytoplasm, both from antibodies [23,31,32,38,48] and from C-terminal proteolysis by carboxypeptidase [44], is also extensive and conclusive. Contrary evidence from pyridoxal phosphate labelling was subsequently shown to be artefactual [33]. Only a single antibody experiment has given an unexplained extracellular location [28].

We are left with the locations of the two short loops L_{89} and $L_{9,10}$ for which evidence is sparse and conflicting. On the one hand, tryptic cleavage sites in L89 were accessible from the cytoplasmic face [20,41] in both the Ca^{2+}- and H^+/K^+-ATPases. On the other hand, epitopes inserted into L_{89} and $L_{9,10}$ of Na^+/K^+-ATPase [30] were found to be extracellular and cytoplasmic, respectively, supporting the 8-segment model in Fig. 2b. The proteolytic experiments [20,41], however, suggested that both L_{89} and $L_{9,10}$ were accessible from the cytoplasm, implying a different 8-segment model in which M9 and M10 are both located there; in the case of Ca^{2+}-ATPase, M9 seems to be membrane associated because it is retained by the membrane after proteolysis. These results not only conflict with each other, but also with two comprehensive studies using expression techniques [43,47].

In the first of these studies [47], the Mg^{2+} pump of *S. typhimurium* was expressed in a series of truncated forms with β-lactamase or β-galactosidase fused as a marker protein to the C-terminal residue. Sixteen of 35 fusion sites were located either in the short extramembranous loops (9 in all, including N and C terminus), or within ~ 4 residues of these loops; β-lactamase or β-galactosidase activity was then used to determine the sidedness of the loops. Only one fusion in L67 gave results inconsistent with the 10-segment model, but two other fusions in L67

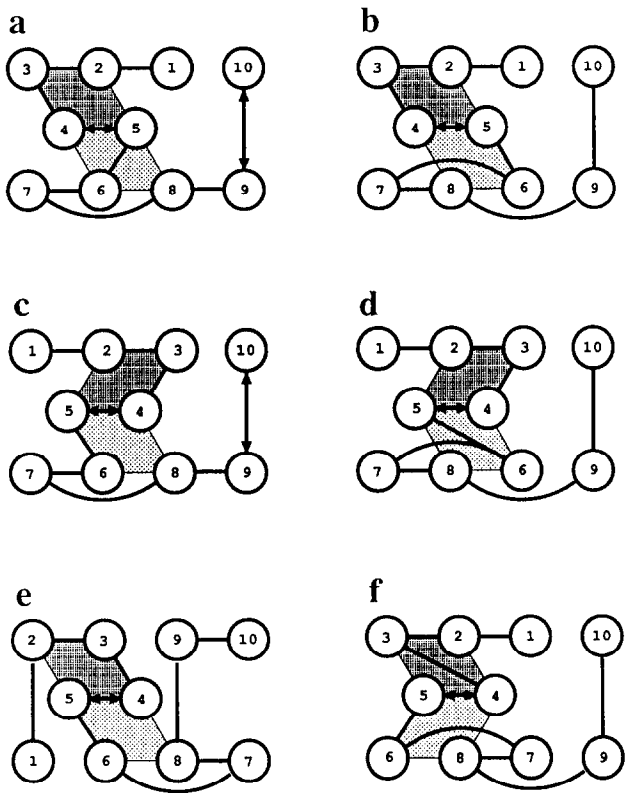

Fig. 4. Analysis of possible folds. Helices were located on a hexagonal grid approximating the shape of the observed electron density. All possible folds were generated in which (1) loops on a given side of the membrane (cytoplasmic or luminal) did not cross one another, (2) no connection was longer than two grid units and (3) short loops (L_{12}, L_{34}, L_{56}, and $L_{9,10}$) were shorter than two grid units. In addition, two further criteria were applied: M2, M3, M4, and M5 should form a bundle (dark grey shading) to lie beneath the stalk and M4, M5, M6, M8 should be packed together to form an ion-binding site (light grey shading). Of the possible 14,833 folds (excluding mirror images which are indistinguishable), 38 satisfied the above requirements. Using the method of Taylor et al. [51], these folds were ranked according to their exposure of variable helices and burial of conserved helices as determined by Green [50] and shown in Fig. 3c. Based on the variability within the Na^+/K^+-ATPase family, the 6 top-scoring folds were thus ranked from a to f. Based on the variability within the Ca^{2+}-ATPase, the folds were ranked b, a, f, d, c, with fold e falling out of the top 6. The top three folds for Ca^{2+}-ATPase (b, a, f) all place the stalk helices in the correct position relative to the reconstruction and also locate M1 underneath the platform. Of these folds, f also places the longest helix, M7, within the sloping lobe B. The double-headed arrows indicate that exchanging the two helices does not affect the overall score. Of the two variants on fold f, the one shown was preferred as it gives a shorter distance for L_{56}.

were consistent with the expected cytoplasmic location of this loop. Aside from this one inconsistency and some ambiguous results from several fusions in the middle of transmembrane segments, this work is uniquely consistent with the 10 transmembrane segments shown in Fig 2a. Unfortunately, the method is only applicable to bacterial expression systems and so cannot at present be used on other P-type pumps. However, the second study ([43]; Bamberg and Sachs, pesonal communication) used in vitro translation of fusion proteins to address the ability of individual transmembrane segments to pass through the membrane, acting either as signal anchor or stop transfer sequences; glycosylation of a sequence fused onto the C-terminus was used to detect sidedness of this C-terminus. When applied to H^+/K^+-ATPase, segments 1,2,3, and 4 inserted nicely into the membrane during translation, as did segments 8,9, and 10. Segments 5,6, and 7 were problematic and the authors suggested that they may not co-insert during translation, but may involve a different, posttranslational insertion. Given strong independent evidence for transmembrane location of segments 5,6, and 7, these results are again consistent with a 10-segment topology.

4. Hypothetical packing of 10 transmembrane helices

Additional support for the 10-segment model came from our attempts to fit 10 helices into the density map of Ca^{2+}-ATPase (Stokes, Taylor and Green, unpublished results). As a first step towards this fit, it was necessary to define the molecular boundary more precisely. Because the contrast within the membrane was low, we calculated the expected volume of the cytoplasmic domains (654 residues yielding 87,192 $Å^3$) and chose a density cut-off for the reconstruction which closely corresponded to this volume (98.7%); this cut-off was then used to generate a molecular envelope within the membrane and actually generated a volume for the whole molecule that was 100.7% of that expected. To determine an appropriate position for helical backbones relative to the boundary of density, we examined the well-determined structure of bacteriorhodopsin [1], which had been truncated to 15 Å resolution by applying a large temperature factor (B = 2070 attenuates data at 15 Å by 90%). At this resolution, the C-α backbone of the 7 helices of bacteriorhodopsin were right up against the molecular envelope (Fig. 3b), indicating that aliphatic and aromatic side chains do not generate much contrast with respect to aliphatic lipid tails at this low resolution. Given these guidelines, we were able to fit 10 helices comfortably into the transmembrane envelope of Ca^{2+}-ATPase (Fig. 3a), whereas an 8 helix model would have left a lot of empty space. In particular, the relative sizes of the A,B and C lobes (defined in Fig. 1) suggested that they contained 6, 2 and 2 helices, respectively.

In order to assign individual helices in this model, we applied constraints provided by mutagenesis and structural connectivity and the results are shown in Fig. 3c. Because one side of the A lobe (A1) lies immediately beneath the stalk, we filled it with helices M2, M3, M4 and M5. Near the membrane surface, the stalk extends into a 'platform', which partly overlies lobe C, and we therefore fitted the 56 residue N-terminal segment into this platform and fitted M1 into lobe C (c.f. [17]). The long M7 helix was fitted into the highly inclined B lobe and M8 into the other side of the A lobe (A2); this is consistent with the position of the lumenal domain, which must contain the long, antigenic lumenal loop (L78) and which clearly links B to A2. We also put M6 into the A2 lobe such that M4, M5, M6, and M8 could cluster together to form the Ca^{2+} site. This leaves M9 to go into the B lobe and M10 to accompany M1 in the C lobe; a tenuous connection between B and C lobes is seen in the map and could represent L9,10.

These assignments are consistent with a theoretical analysis of Ca^{2+}-ATPase regarding both the distribution of variable residues around the putative transmembrane helices [50] and their possible arrangements [51]. In all but the three most highly conserved helices (M4, M5, M6), the variable residues were clustered on one face of each helix, thus defining a surface likely to be exposed to the lipid [52]. This surface helped to define both the location and the azimuth of the helix within the low resolution structure as follows. Many possible arrangements of the 10 helices were generated and ranked according to the exposure of individual helices to the lipid environment. The six most probable arrangements are shown in Fig. 4, in which Fig. 4f (ranked third most probable) corresponds to the arrangement in Fig. 3c. Although these results were obtained with Ca^{2+}-ATPase, it is also noteworthy that the family of Na^+/K^+-ATPase sequences showed a similar distribution of variable sites, even though the mean pairwise identity between the two families was only 20% in the transmembrane region, and generated a very similar ranking of helix arrangements (Fig. 4) As expected, M4 is deeply buried, both because of its high conservation and because of the results of site directed mutagenesis [53], which showed large effects on activity from mutations located all around this helix. Also, the highly variable M3, M9 and M10 are all in exposed positions. The exposed position of M6 is less satisfying, because of its high conservation, but we settled on this arrangement in order to avoid both a long distance between M8 and M9 and a short M5–M6 connection diagonally across the entrance to the Ca^{2+} site. This, together with the somewhat irregular path of the inter-helix connections, are the least satisfactory aspects of the model, which otherwise satisfies the complex pattern of constraints. We hope that this model will suggest a number of experimental tests, the results of which will undoubtedly lead to future refinements.

Acknowledgements: We would like to acknowledge Richard Henderson for providing structure factors and atomic coordinates for bacteriorhodopsin.

References

[1] Henderson, R., Baldwin, J.M., Ceska, T.A., Zemlin, F., Beckmann, E. and Downing, K.H. (1990) J. Mol. Biol. 213, 899–929.
[2] Skriver, E., Maunsbach, A.B. and Jorgensen, P.L. (1981) FEBS Lett. 131, 219–222.
[3] Dux, L. and Martonosi, A. (1983) J. Biol. Chem. 258, 2599–2603.
[4] Castellani, L., Hardwicke, P.M. and Vibert, P. (1985) J. Mol. Biol. 185, 579–594.
[5] Taylor, K.A., Dux, L. and Martonosi, A. (1986) J. Mol. Biol. 187, 417–427.
[6] Ovchinnikov, Y.A., Demin, V.V., Barnakov, A.N., Kuzin, A.P., Lunev, A.V., Modyanov, N.N. and Dzhandzhugazyan, K.N. (1985) FEBS Lett. 190, 73–76.
[7] Mohraz, M., Simpson, M.V. and Smith, P.R. (1987) J. Cell Biol. 105, 1–8.
[8] Hebert, H., Skriver, E. and Maunsbach, A.B. (1985) FEBS Lett. 187, 182–186.
[9] Hebert, H., Skriver, E., Soderholm, M. and Maunsbach, A.B. (1988) J. Ultrastruct. Mol. Struct. Res. 100, 86–93.
[10] Herbette, L., DeFoor, P., Fleischer, S., Pascolini, D., Scarpa, A. and Blasie, J.K. (1985) Biochim. Biophys. Acta 817, 103–122.
[11] Skriver, E., Kaveus, U., Hebert, H. and Maunsbach, A.B. (1992) J. Struc. Biol. 108, 176–185.
[12] Tahara, Y., Ohnishi, S., Fujiyoshi, Y., Kimura, Y. and Hayashi, Y. (1993) FEBS Lett. 320, 17–22.
[13] Dux, L., Pikula, S., Mullner, N. and Martonosi, A. (1987) J. Biol. Chem. 262, 6439–6442.
[14] Taylor, K.A., Mullner, N., Pikula, S., Dux, L., Peracchia, C., Varga, S. and Martonosi, A. (1988) J. Biol. Chem. 263, 5287–5294.
[15] Stokes, D.L. and Green, N.M. (1990) J. Mol. Biol. 213, 529–538.
[16] Stokes, D.L. and Lacapere, J.-J. (1994) J. Biol. Chem. 269, in press.
[17] Toyoshima, C., Sasabe, H. and Stokes, D.L. (1993) Nature 362, 469–471.
[18] Taylor, K.A., Ho, M.H. and Martonosi, A. (1986) Ann. N.Y. Acad. Sci. 483, 31–43.
[19] MacLennan, D.H., Brandl, C.J., Korczak, B. and Green, N.M. (1985) Nature 316, 696–700.
[20] Sachs, G., Shin, J.M., Besancon, M., Munson, K. and Hersey, S. (1992) Ann. N.Y. Acad. Sci. 671, 204–216.
[21] Matthews, I., Sharma, R.P., Lee, A.G. and East, J.M. (1990) J. Biol. Chem. 265, 18737–18740.
[22] Moller, J.V., Juul, B., Lee, Y.-J., leMaire, M. and Champeil, P. (1994) in: The Sodium Pump: Structure, Mechanisms, Hormonal Control and Its Role in Disease (Schoner, W. and Bamberg, E., Eds.) Steinkopff Verlag, Darmstadt, in press.
[23] Matthews, I., Colyer, J., Mata, A.M., Green, N.M., Sharma, R.P., Lee, A.G. and East, J.M. (1989) Biochem. Biophys. Res. Commun. 161, 683–688.
[24] Clarke, D.M., Loo, T.W. and MacLennan, D.H. (1990) J. Biol. Chem. 265, 17405–17408.
[25] Mata, A., Matthews, I., Tunwell, R.E.A., Sharma, R.P., Lee, A.G. and East, J.M. (1992) Biochem. J. 286, 567–580.
[26] Capasso, J.M., Hoving, S., Tal, D.M., Goldshleger, R. and Karlish, S.J.D. (1992) J. Biol. Chem. 267, 1150–1158.
[27] Karlish, S.J.D., Goldshleger, R. and Jorgensen, P.L. (1993) J. Biol. Chem. 268, 3471–3478.
[28] Ovchinnikov, Y.A., Luneva, N.M., Arystarkhova, E.A., Gevondyan, N.M., Arzamazova, N.M., Kozhich, A.T., Nesmeyanov, V.A. and Modyanov, N.N. (1988) FEBS Lett. 227, 230–234.
[29] Mohraz, M., Arystarkhova, E.A. and Sweadner, K.J. (1994) J. Biol. Chem. 269, 2929–2936.
[30] Canfield, V.A. and Levenson, R. (1993) Biochemistry 32, 13782–13786.
[31] Ning, G., Maunsbach, A.B., Lee, Y.-J. and Moller, J.V. (1993) FEBS Lett. 336, 521–524.
[32] Antolovic, R., Brüller, H.-J., Bunk, S., Linder, D. and Schoner, W. (1991) Eur. J. Biochem. 199, 195–202.
[33] Thibault, D. (1993) Biochemistry 32, 2813–2821.
[34] Modyanov, N.N., Vladimirova, N.M., Gulyaev, D.I. and Efremov, R.G. (1992) Ann. N.Y. Acad. Sci. 671, 134–146.
[35] Price, E.M. and Lingrel, J.B. (1993) Biochemistry 27, 8400–8408.
[36] Schultheis, P.J., Wallick, E.T. and Lingrel, J.B. (1993) J. Biol. Chem. 268, 22686–22694.
[37] Kano, I., Satoh, K., Nagai, F., Ushiyama, K., Nakao, T., Hara, Y. and Kano, K. (1990) Biochem. Cell Biol. 68, 1262–1267.
[38] Mercier, F., Bayle, D., Besancon, M., Joys, T., Shin, J.M., Lewin, M.J.M., Prinz, C., Reuben, M.A., Soumarmon, A., Wong, H., Walsh, J.H. and Sachs, G. (1993) Biochim. Biophys. Acta 1149, 151–165.
[39] Bamberg, K., Mercier, F., Reuben, M.A., Kobayashi, Y., Munson, K.B. and Sachs, G. (1992) Biochim. Biophys. Acta 1131, 69–77.
[40] Munson, K.B., Gutierrez, C., Balaji, V.N., Ramnarayan, K. and Sachs, G. (1991) J. Biol. Chem. 266, 18976–18988.
[41] Besancon, M., Shin, J.M., Mercier, F., Munson, K., Miller, M., Hersey, S. and Sachs, G. (1993) Biochemistry 32, 2345–2355.
[42] Shin, J.M., Besancon, M., Simon, A. and Sachs, G. (1993) Biochim. Biophys. Acta 1148, 223–233.
[43] Bamberg, K. and Sachs, G. (1993) Mol. Biol. Cell 4, 311a.
[44] Scott, D.R., Munson, K., Modyanov, N. and Sachs, G. (1992) Biochim. Biophys. Acta 1112, 246–250.
[45] Adamo, H.P., Caride, A.J. and Penniston, J.T. (1992) J. Biol. Chem. 267, 14244–14249.
[46] Feschenko, M.S., Avaritch, E.I., Hofmann, F., Shakhparonov, M.I., Modyanov, N.N., Vorherr, T. and Carafoli, E. (1992) J. Biol. Chem. 267, 4097–4101.
[47] Smith, D.L., Tao, T. and Maguire, M.E. (1993) J. Biol. Chem. 268, 22469–22479.
[48] Mandala, S.M. and Slayman, C.W. (1989) J. Biol. Chem. 264, 16276–16281.
[49] Hennessey, J.P. and Scarborough, G.A. (1990) J. Biol. Chem. 265, 532–537.
[50] Green, N.M. (1994) in: The Sodium Pump: Structure, Mechanisms, Hormonal Control and Its Role in Disease (Bamberg, E. and Schoner, W., Eds.) Steinkopff Verlag, Darmstadt, in press.
[51] Taylor, W.R., Jones, D.T. and Green, N.M. (1994) Proteins 18, 281–294.
[52] Baldwin, J.M. (1993) EMBO J. 12, 1693–1703.
[53] Clarke, D.M., Loo, T.W., Rice, W.J., Andersen, J.P., Vilsen, B. and MacLennan, D.H. (1993) J. Biol. Chem. 268, 18359–18364.
[54] Clarke, D.M., Loo, T.W., Inesi, G. and MacLennan, D.H. (1989) Nature 339, 476–478.